Hindawi
Journal of Chemistry
Volume 2017, Article ID 5849103, 10 pages
https://doi.org/10.1155/2017/5849103

Research Article

Synthesis and Characterization of Ag-Modified V_2O_5 Photocatalytic Materials

Dora Alicia Solis-Casados,[1] Luis Escobar-Alarcon,[2] Antonia Infantes-Molina,[3] Tatyana Klimova,[4] Lizbeth Serrato-Garcia,[1] Enrique Rodriguez-Castellon,[3] Susana Hernandez-Lopez,[5] and Alejandro Dorazco-Gonzalez[1]

[1]*Centro Conjunto de Investigación en Química Sustentable UAEM-UNAM, Km 14.5 Carretera Toluca-Atlacomulco, Unidad San Cayetano, 50200 Toluca, MEX, Mexico*
[2]*Departamento de Física, Instituto Nacional de Investigaciones Nucleares, P.O. Box 18-1027, 11801 Mexico City, Mexico*
[3]*Departamento de Quimica Inorganica, Facultad de Ciencias, Universidad de Malaga, 29071 Malaga, Spain*
[4]*Departamento de Ingenieria Quimica, UNAM, Mexico City, Mexico*
[5]*Facultad de Química, Universidad Autónoma del Estado de México, Paseo Colon esq Paseo Tollocan Col Nueva la Moderna, 50000 Toluca, MEX, Mexico*

Correspondence should be addressed to Dora Alicia Solis-Casados; solis_casados@yahoo.com.mx

Received 6 August 2016; Revised 29 October 2016; Accepted 10 November 2016; Published 14 February 2017

Academic Editor: Julie J. M. Mesa

V_2O_5 powders modified with different theoretical silver contents (1, 5, 10, 15, and 20 wt% as Ag_2O) were obtained with acicular morphologies observed by scanning electron microscopy (SEM). Shcherbinaite crystalline phase is transformed into the $Ag_{0.33}V_2O_5$ crystalline one with the incorporation and increase in silver content as was suggested by X-ray diffraction (XRD) and X-ray photoelectron spectroscopy (XPS) analysis. With further increase in silver contents the Ag_2O phase appears. Catalysts were active in photocatalytic degradation of malachite green dye under simulated solar light, which is one of the most remarkable facts of this work. It was found that V_2O_5-20Ag was the most active catalytic formulation and its activity was attributed to the mixture of coupled semiconductors that promotes the slight decrease in the rate of the electron-hole pair recombination.

1. Introduction

In recent years, wastewaters from domestic and industrial uses have contributed to the environmental problem because they arrive to the soil and aquifers mantles polluting clean water. In order to address this issue, the effort of many researchers from several scientific disciplines around the world [1, 2] has been focused on wastewater remediation. Heavy metals such as mercury, iron, cadmium, and chromium are included between the most dangerous pollutants in wastewaters as well as some organic compounds such as the phenols, dyes, pesticides, pharmaceutical, and fertilizers and in some cases solvents. All of them are extremely toxic to the humans and also living organisms, even if they are in a low concentration [3]. Several researchers have proposed solutions to reduce the most dangerous and toxic pollutants contained in wastewaters and also to improve water quality modifying the chemical processes, proposing new absorbent materials and some of the advanced oxidation processes as photocatalysis, which includes developing a photocatalytic material. The remotion of the most resilient organic compounds is among the most important topics concerning wastewater remediation and widely studied nowadays. In so many cases, one of the most extended methods is the photocatalytic degradation, whereby the catalyst is activated by using light. It is noteworthy that degradation of the resilient organic compounds dissolved in water occurs in a natural way by the photolysis process by using the cheapest

source energy such as that provided by the sun. The main disadvantage is its very low efficiency since the organic molecules degrade slowly, taking days and even months to achieve the complete mineralization of organic compounds into water and CO_2. The photocatalytic process increases the decomposition rate of organic compounds present in wastewaters. The photocatalyst employed is commonly a semiconductor material with desirable characteristics such as photoactivity, being chemically and biologically inert, photostability, nontoxicity, and low cost [4]. A photocatalyst could be employed in its pure, mixed, or doped form. An example of this is the TiO_2 in its anatase crystalline phase with a band gap energy around 3.2 eV and the rutile crystalline phase with a band gap energy of 3.0 eV [5, 6]. It has been reported that mixing different ratios of anatase : rutile results in higher catalytic activities, which can be attributed to the synergistic effect between both phases, as occurs in coupled semiconductors [7]. Titania in its anatase crystalline phase is in disadvantage for generating the electron-hole pair if the excitation source is sunlight [8, 9]. It is the reason to improve the photocatalytic performance of TiO_2 by doping and modification with metals and nonmetals [10, 11]. It is well known that, in order to obtain better catalytic performance, it is not enough that the photocatalytic material has a low band gap energy to be active under sunlight. Some unstable materials with reduced band gap energy are Fe_2O_3 (2.3 eV), GaP (2.23 eV), and GaAs (1.4 eV) that are not so good as photocatalysts to degrade organic compounds in aqueous solutions [12]. It has been reported before by some researchers that one of the materials with low band gap energy, of around 2.8 eV, and some stability in aqueous solutions is the V_2O_5-based photocatalysts [13], potentially active under irradiation with visible light and investigated in the last years [14–17]. The synthesis of V_2O_5 has been reported by using techniques as the hydrothermal synthesis [18], sol-gel technique [19], thermal decomposition of several precursors as ammonium metavanadate (NH_4VO_3) [20], flame-spray pyrolysis [21, 22] magnetron sputtering, electron-beam evaporation, and pulsed laser deposition [23, 24], obtaining several morphologies as nanobelts [18, 19], nanowires [18], nanoribbons, nanopowders [18, 21], and also thin films [19, 21–23]. Thin films and powders have been obtained with different textural and structural properties related in some cases with their photocatalytic activity [24–26]. It should be considered that the request of doped or coupled a V_2O_5 catalyst to another semiconductor to retarding the recombination of the electron-hole pair, improving catalytic activity [27], is due to the disadvantage of short migration distances for excited electron-hole pairs which increases the recombination rate and decreasing the photocatalytic activity. Other researchers to solve this fact in photocatalysts with low band gap energy have reported that adding a small amount of noble metals (such as Pt, Ag, and Pd) [28–30] could retard the recombination of the electron-hole pair and increase the photocatalytic activity of the V_2O_5. In this research work, the synthesis of Ag-modified V_2O_5 photocatalytic materials through the surfactant assisted technique by using the non-ionic surfactant molecule polyoxyethylene lauryl ether (Brij L23) is proposed. The main purpose was to obtain catalytic formulations based in V_2O_5-xAg that could be photoactive to degrade organic compounds contained in water under simulated solar light.

2. Experimental

2.1. Synthesis of V_2O_5 and Ag-Modified V_2O_5 Photocatalysts. V_2O_5 powders from Fermont were treated by the surfactant assisted technique. This technique uses a micellar solution prepared using polyoxyethylene (23) lauryl ether ($C_{12}E_{23}$, Brij L23 30% w/v solution from Sigma Aldrich), dibutyl ether ($[CH_3(CH_2)_3]_2O$, DBE-reagent plus ≥99% from Sigma Aldrich), and $AgNO_3$ (ACS Reagent, ≥99.0% from Sigma Aldrich). To obtain V_2O_5 photocatalyst, the commercial V_2O_5 was added to the micellar solution previously prepared with 30% Brij L23, 10% DBE, and 60% of water, solvothermally pressurized in a reactor at 60°C for 12 hours, with slow stirring. The obtained solids were filtered, washed with deionized water, and then thermally treated, raising temperature from room temperature to 400°C, at a heating rate of 5°C/min; afterwards, the temperature was isothermally maintained at 400°C for 3 hours in an air convection oven to eliminate the surfactant Brij L23; this sample was called hereinafter V_2O_5. The Ag-modified V_2O_5 photocatalysts were prepared by following the same synthesis procedure. Thus, the required amounts of V_2O_5 and $AgNO_3$ precursors were added to the micellar solution of Brij L23 to obtain a theoretical content of 1, 5, 10, 15, and 20 wt.% of Ag_2O. Photocatalysts will be referred hereinafter as V_2O_5-xAg, where x represents the percentage in weight of Ag_2O (1, 5, 10, 15, and 20 wt% Ag_2O) and for simplicity the Ag_2O content in some parts of the manuscript has been referred as the Ag load.

2.2. Physicochemical Characterization of V_2O_5-xAg. The temperature of surfactant elimination to obtain the photocatalytic formulation was determined from thermogravimetry and differential scanning calorimeter analysis (TGA-DSC), performed by using a Netzsch, STA 449 F3 Jupiter equipment. The weight loss and the heat flow during decomposition were measured in flowing air (20 mL/min) and heating from room temperature to 600°C at a heating rate of 3°C/min. Molecular structure was studied through the infrared spectra (IR) acquired in a Bruker tensor 27 IR spectrometer with ATR accessory. Surface morphology was observed with scanning electron microscopy (SEM) by using a JEOL JSM 6510 LV microscope; additionally, compositional analysis was carried out with an acceleration voltage of 15 kV, using an EDS probe coupled to the same microscope. Raman spectra (RS) were acquired using an HR LabRam 800 system equipped with an Olympus BX40 confocal microscope; a Nd:YAG laser beam (532 nm) was focused by a 100x objective onto the sample surface. A cooled CCD camera was used to record the spectra, usually averaged for 100 accumulations of 10 seconds in order to improve the signal-noise ratio. All spectra were calibrated using the 521 cm^{-1} line of monocrystalline silicon. X-ray diffraction (XRD) patterns were obtained with a X'Pert PRO MPD Philips diffractometer (PANanalytical), using monochromatic CuKα radiation ($\lambda = 1.5406$ Å). The Kα radiation was selected with a Ge (1 1 1) primary monochromator. The X-ray tube was set at 45 kV and 40 mA. X-ray diffraction (XRD) measurements were also performed on a

Rigaku D/MAX III B diffractometer with a copper target. X-ray line broadening analysis (XLBA) was performed using computer software supplied by Rigaku after measurement in the step scan mode. The textural properties (S_{BET}, Vp, and dp) were measured from the nitrogen adsorption-desorption isotherms at −196°C by an automatic ASAP 2020 system from Micromeritics. Prior to the measurements, samples were outgassed at 200°C and 10^{-4} mbar overnight. Surface areas were determined by using the Brunauer-Emmett-Teller (BET) equation and a nitrogen diatomic molecule cross section of 16.2 Å^2. The total pore volume was calculated from the adsorption isotherm at $P/P_0 = 0.996$. The optical band gap energy (E_g) values were determined using the Kubelka-Munk method; this was done by transforming the reflectance spectra of the samples with different Ag contents to the Kubelka-Munk function, $F(R)$, and then plotting $(F(R)E)^{1/2}$ versus E. The values of Eg were obtained by a linear fit at linear segments of the curve, determining its intersection with the photon energy axis [32]. It was mentioned in [33] that there are some discrepancies in opinion about the Kubelka-Munk method, but it is used with the sufficient accuracy required in photocatalytic applications. With the maximum absorbance in the UV-Vis spectra, it was observed the excitation wavelength of each sample to emit photoluminescence; this maximum has a slight shift; thus emission spectra were obtained with an excitation source fixed at $\lambda = 492$ nm in a FluoroMax-4, HORIBA, Jobin Yvon fluorometer. The intensity of the emission spectrum seems to be related to the rate of electron-hole recombination [34]. X-ray photoelectron spectra (XPS) were collected using a Physical Electronics PHI 5700 spectrometer with nonmonochromatic Mg Kα radiation (300 W, 15 kV, and 1256.6 eV) with a multichannel detector. Survey spectra were recorded from 0 to 1000 eV at constant pass energy of 100 eV, onto 720 μm diameter analysis area; narrow spectra of samples were recorded in the constant pass energy mode at 20 eV, using a 720 μm diameter analysis area and 10 scans at least. Charge correction was adjusted by using the carbon signal (C 1*s* at 285 eV). A PHI ACCESS ESCA-V6.0 F software package was used for acquisition and data analysis. A Shirley type background was subtracted from the spectra and then they were fitted using Gaussian-Lorentzian curves to determine the binding energies of the different element core levels more accurately. NIST database was used to identify the corresponding element to the measured binding energies.

2.3. Photocatalytic Activity Tests. The photocatalytic activity of the V_2O_5-*x*Ag photocatalysts was evaluated through the degradation reaction of a model molecule as the malachite green (MG) dye ($C_{23}H_{26}N_2O$) using an aqueous solution of 10 μmol/l. For this purpose, 0.05 g of catalyst was added to a batch reaction system and stirred in a dark room until reaching the adsorption equilibrium. Catalysts were activated by illumination with a solar simulator SF-150B class ABA from Sciencetech, emitting 6% of UV radiation. The light source was placed at a height of 40 cm from the solution surface. The degradation reaction was monitored by the decrease in intensity of the characteristic absorption band of the MG peaking at 619 nm in the UV-Vis spectra. Reaction was followed by 3 hours taking aliquots every 15 minutes. The obtained absorbances at each reaction time were correlated to MG concentrations through a calibration curve traced previously. The kinetic trace at 619 nm is related mainly to the MG concentration change. This trace could be fitted to a pseudo-first-order expression (exponential curve) with acceptable precision to determine the rate constant (k_{app}). Total organic carbon (TOC) was determined by the combustion method, for each solution at the end of the corresponding reaction as ppm of carbon. The mineralization degree was calculated taking as the percent from $[(T_{initial} - T_{final})/T_{initial}]$, where T_{final} and $T_{initial}$ are the TOC values at the end of the reaction and of the original solution, respectively.

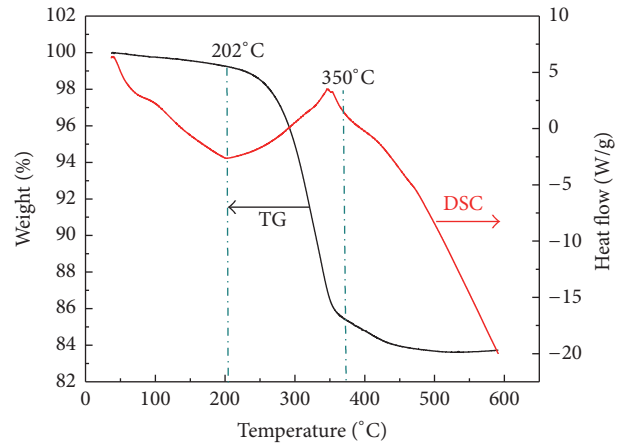

FIGURE 1: TGA-DSC curves of V_2O_5 catalyst precursor.

3. Results and Discussion

3.1. Surfactant Elimination

3.1.1. Thermal Analysis and Infrared Spectroscopy of V_2O_5 Precursors. From TGA-DSC curves shown in Figure 1, the temperature to eliminate the surfactant Brij L23 from V_2O_5 catalyst precursor was determined. The TGA curve shows a main weight loss starting at 200°C and finishing at 450°C, accompanied with an exothermic peak (DSC curve) at 350°C that can be attributed to the thermal decomposition of the surfactant [35]. The incorporation and further increase of Ag promotes a slight decrease in the exothermic peak temperature until 340°C. Therefore, the thermal treatment was carried out at 400°C for 3 hours, in order to achieve the elimination of the surfactant and to favor the thermal decomposition of the $AgNO_3$ into Ag_2O and also to induce the crystallization of the catalytic formulation. To confirm if the organic material was removed after the thermal treatment, IR spectra of V_2O_5-*x*Ag photocatalysts, before and after the thermal treatment, were compared; the results will be discussed later.

3.2. Surface Properties

3.2.1. Scanning Electron Microscopy. The morphology of the V_2O_5-*x*Ag photocatalysts was observed from the SEM images shown in Figures 2(a)–2(d). It is clear that silver

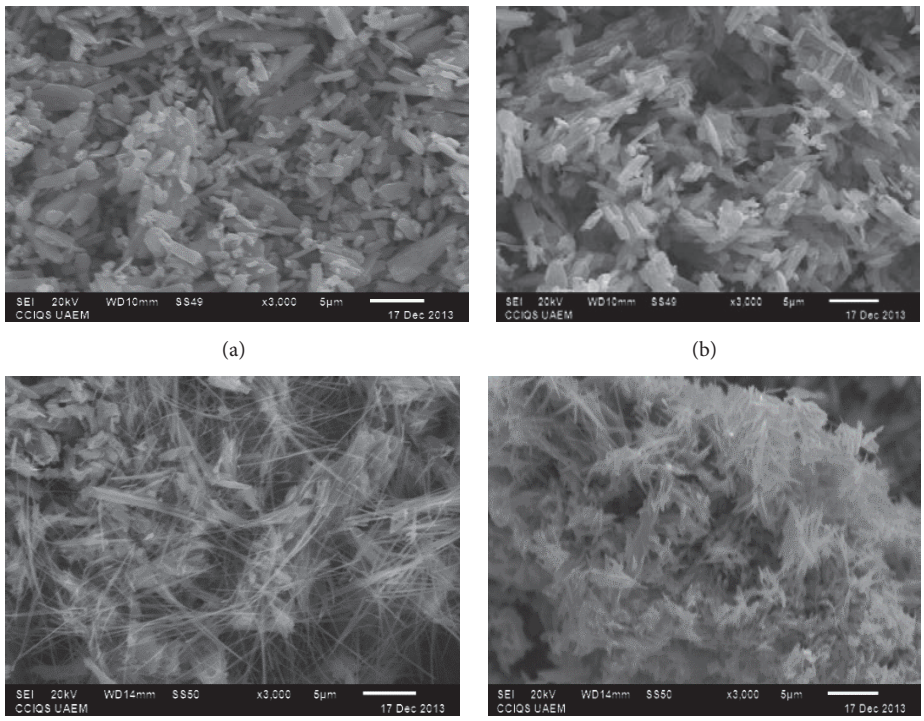

Figure 2: Scanning electron microscopy images at 3000x of (a) V_2O_5, (b) V_2O_5-5Ag, (c) V_2O_5-10Ag, and (d) V_2O_5-20Ag photocatalysts.

incorporation into the photocatalytic formulation changes morphology, obtaining acicular forms, which begin with the morphology bar-type with lengths about 2-3 microns as can be seen in Figures 2(a) and 2(b) for V_2O_5 and V_2O_5-5Ag photocatalysts. Further increase in silver content in the catalytic formulation promotes changes in the morphology, obtaining wires as can be seen in Figures 2(c) and 2(d) for V_2O_5-10Ag and some sharped bars in V_2O_5-20Ag photocatalysts. The catalytic performance observed for each formulation could be associated with the morphology as some changes are expected in textural properties related to morphology. It seems that nucleation process generates crystallites with different morphologies when silver is incorporated into the photocatalytic formulation. That process could be attributed to the solvothermal synthesis procedure mainly and to the increase in Ag_2O load to form different crystalline phases that have different crystallographic data. Elemental atomic composition % in the catalytic surface was determined by the EDS analysis, values shown in Table 1. The atomic % of Ag content increases as was expected with the increase in the theoretical Ag_2O content.

3.2.2. N_2-Physisorption Measurements. Textural properties, such as the specific surface area and total pore volume, were studied using the N_2 physisorption technique. This was done to estimate the effect of the changes observed in the morphology of the V_2O_5-xAg photocatalysts, on their surface properties. The specific surface area values, calculated using the BET model, are included in Table 2. These values increase with the Ag_2O content, from 5.3 to 14.6 m^2/g, which represent an increase close to 300%. These data indicate that Ag_2O incorporation increases the specific surface area and the porosity compared with pure V_2O_5. This result could be explained in terms of a higher amount of empty spaces between the formed particles with narrow dimensions as was observed in the SEM images. N_2-physisorption isotherms are shown in Figure 3, which according to IUPAC are type II, characteristic of low porous solids presenting meso- and macroporosity. An increase in the nitrogen adsorption volume with the increase of the silver content in the catalytic formulation is clear from the isotherms. A small hysteresis loop is observed, attributed to the empty spaces between particles with irregular forms and sizes.

Table 1: Comparison of atomic percent of silver in V_2O_5-xAg photocatalysts measured by XPS and EDS.

	Ag content (at.%) (XPS)	Ag content (at.%) (SEM)
V_2O_5	—	—
V_2O_5-1Ag	1.5	1.1
V_2O_5-5Ag	2.9	1.3
V_2O_5-10Ag	4.5	4.3
V_2O_5-15Ag	4.5	5.1
V_2O_5-20Ag	6.8	8.1

3.3. Crystalline and Molecular Structures

3.3.1. X-Ray Powder Diffraction. Figure 4 shows the diffractograms of the V_2O_5-xAg photocatalysts, where the main

Table 2: Specific surface area (S_{BET}) and pore volume (V_p) of pure V_2O_5 and V_2O_5-xAg photocatalysts.

Sample	S_{BET} (m^2/g)	V_p (cm^3/g)
V_2O_5*	3.3	0.005
V_2O_5**	3.4	0.010
V_2O_5-1Ag	5.3	0.020
V_2O_5-5Ag	11.0	0.023
V_2O_5-10Ag	10.6	0.030
V_2O_5-15Ag	11.9	0.025
V_2O_5-20Ag	14.6	0.026

*Commercial.
**Synthesized.

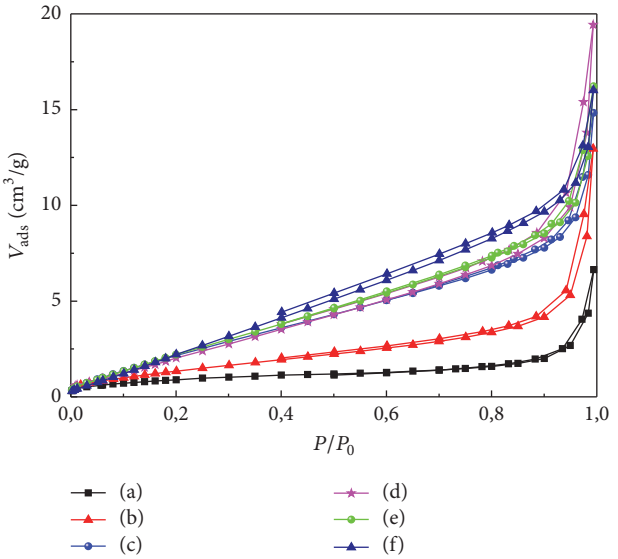

Figure 3: N_2 adsorption-desorption isotherms of (a) V_2O_5, (b) V_2O_5-1Ag, (c) V_2O_5-5Ag, (d) V_2O_5-10Ag, (e) V_2O_5-15Ag, and (f) V_2O_5-20Ag.

crystalline phases such as the Shcherbinaite V_2O_5, the $Ag_{0.33}V_2O_5$ bronze, and the Ag_2O oxide are observed. The intensity in the diffraction lines changes with the increase of the Ag load in the photocatalytic formulation. The diffractogram of the synthesized V_2O_5 catalyst (Figure 4(a)) shows diffraction lines at 2θ = 15.3, 20.2, 21.7, 26.1, 31.0, 32.3, 34.3, 41.2, and 47.3° that characterize unambiguously the Shcherbinaite crystalline phase of V_2O_5 (JCPDS 41-1426). After Ag incorporation, other diffraction lines become noticeable at 2θ = 29.2, 27.8, 30.6, 30.8, and 32.8° in the samples with the V_2O_5-1Ag and V_2O_5-5Ag catalysts. These new signals can be assigned to the called silver vanadium bronzes, specifically to the $Ag_{0.33}V_2O_5$ crystalline structure (JCPDS 81-1740). Further increase in silver load, samples V_2O_5-10Ag and V_2O_5-20Ag, gives rise to the appearance of new diffraction signals at 2θ = 32.9, 38.1, 54.9, and 65.7°, attributed to the Ag_2O crystalline phase (JCPDS 01-1041). These diffraction lines are very weak probably due to a dilution or dispersion effects and to a small crystallite size under 40 Å. It is clear that V_2O_5 crystalline phase almost disappears at the highest silver loads.

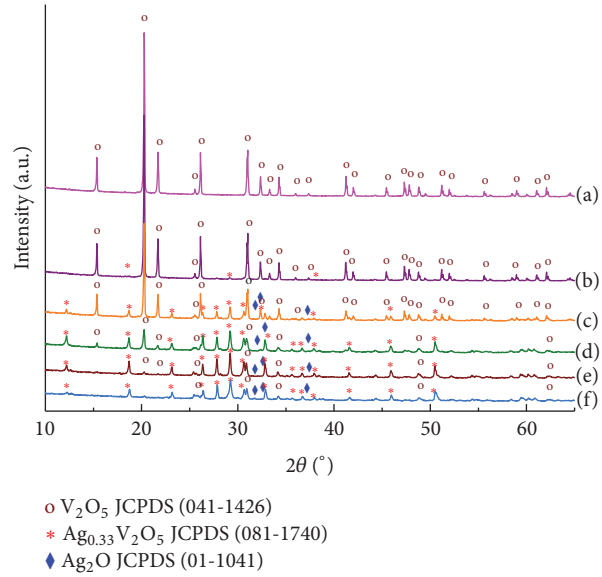

Figure 4: XRD diffraction patterns of (a) V_2O_5, (b) V_2O_5-1Ag, (c) V_2O_5-5Ag, (d) V_2O_5-10Ag, (e) V_2O_5-15Ag, and (f) V_2O_5-20Ag photocatalysts.

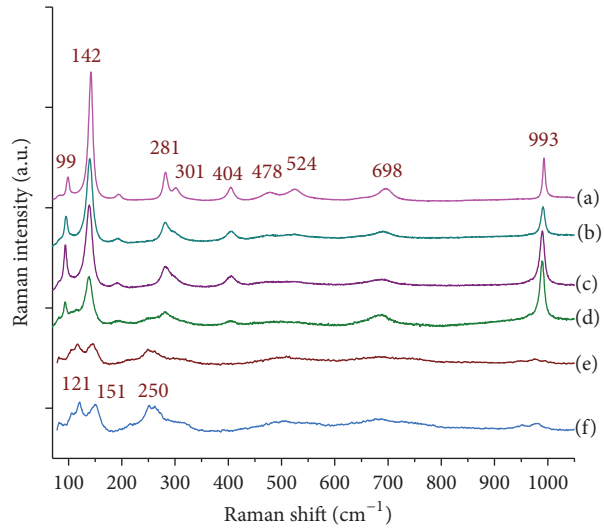

Figure 5: Raman spectra of samples (a) V_2O_5, (b) V_2O_5-1Ag, (c) V_2O_5-5Ag, (d) V_2O_5-10Ag, (e) V_2O_5-15Ag, and (f) V_2O_5-20Ag.

3.3.2. Raman Spectroscopy. To corroborate the microcrystalline structure observed by XRD, Raman spectra of unmodified and Ag-modified V_2O_5 photocatalysts were recorded. It can be seen in the spectra shown in Figure 5 that the Ag incorporation modifies some signals of the Raman spectra with respect to the synthesized V_2O_5 catalyst. The characteristic peaks of the V_2O_5, located at 99, 193, 281, 301, 404, 478, 524, 698, and 993 cm^{-1}, decrease and almost disappear by raising the amount of Ag_2O added during the synthesis along with the appearance of new peaks. The main peak located at 142 cm^{-1}, characteristic of the skeleton bend vibration, shifts from 142 cm^{-1} in V_2O_5 to 138 cm^{-1} in V_2O_5-10Ag photocatalyst, probably due to the distortion of the V_2O_5

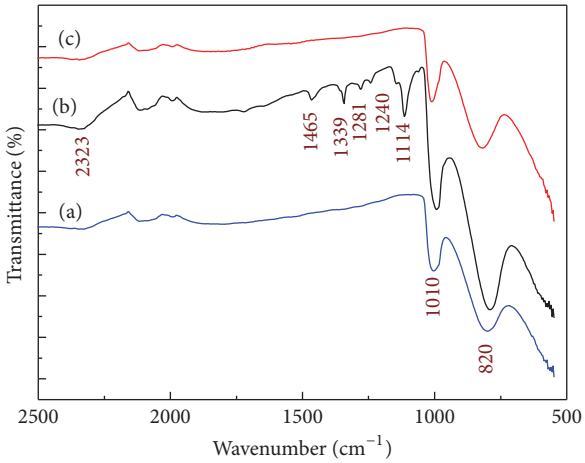

FIGURE 6: Infrared spectra of commercial V_2O_5 (a), V_2O_5 obtained through the surfactant assisted technique before calcination (b), and synthesized V_2O_5 after calcination (c).

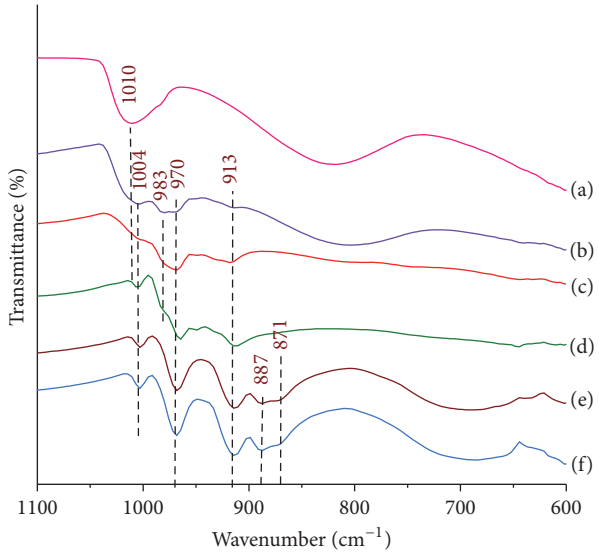

FIGURE 7: IR spectra of (a) V_2O_5, (b) V_2O_5-1Ag, (c) V_2O_5-5Ag, (d) V_2O_5-10Ag, (e) V_2O_5-15Ag, and (f) V_2O_5-20Ag photocatalysts.

structure caused by the Ag incorporation into the V_2O_5 lattice. New Raman bands at 121, 151, and 250 cm^{-1} appear for samples with the highest Ag_2O loads and V_2O_5-15Ag and V_2O_5-20Ag samples, which could be attributed to the formation of the $Ag_{0.33}V_2O_5$ bronze. It is noteworthy that no signals associated with Ag_2O were observed, contrary with the XRD results; this could be attributed to the small Raman section of this compound.

3.3.3. Infrared Spectroscopy. Infrared spectra were recorded with two main purposes: firstly, to corroborate the surfactant elimination from the photocatalytic preparation, as can be seen in Figure 6; secondly, to observe the bond vibration when silver is added at different Ag_2O loads. IR spectra of V_2O_5, commercial and as-synthetized, before and after thermal treatment, were compared. The IR spectrum of the commercial sample shows two bands at 1010 cm^{-1} and 820 cm^{-1} ascribed to the coupled vibration between V=O and V–O–V stretching vibrations [36, 37]. The infrared spectrum of the synthesized V_2O_5 before the thermal treatment also presents IR absorption bands characteristics of the surfactant at 1114, 1240, 1281, 1339, and 1465 cm^{-1} [38], attributed to the C-C and C-H bending in the alkyl groups of the surfactant Brij L23. After thermal treatment, these bands disappear confirming the surfactant elimination. IR spectra of the different V_2O_5-xAg photocatalysts are shown in Figure 7. The incorporation and further increase of the Ag_2O load promote the shift of the band at 1010 cm^{-1} to 1000 cm^{-1} and the disappearance of the band located at 820 cm^{-1} when the theoretical Ag_2O loading is higher than 5 wt.%. The observed shift has been assigned to disordered vacancies in the V_2O_5 lattice [39] due to the presence of Ag. The spectrum of the V_2O_5-1Ag sample shows bond vibrations located at 983 cm^{-1} and 970 cm^{-1}; the last one remains for samples with higher Ag_2O loads. The band at 983 cm^{-1} is related to the decrease of the bond strength of V=O stretch vibration by the incorporation of silver into the photocatalytic formulation as observed for Na-bronzes [40]. New infrared bands, at 917, 890 and 871 cm^{-1} and a broad band at 700 cm^{-1}, appear with the increase in Ag content. These could be ascribed to the presence of the $Ag_{0.33}V_2O_5$ bronze identified by XRD.

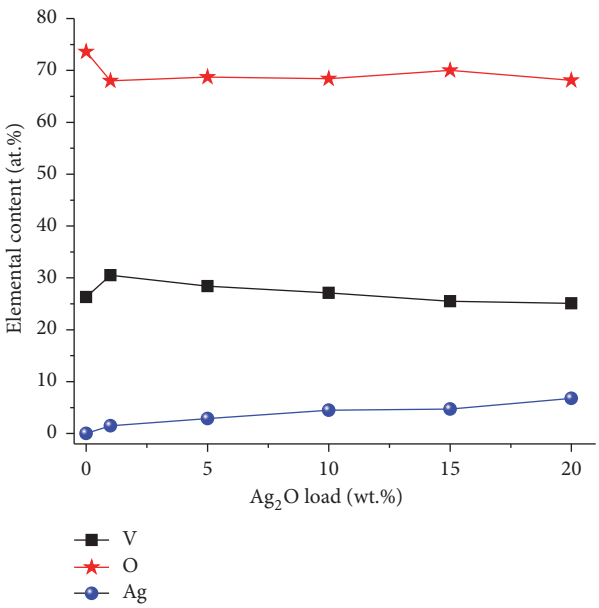

FIGURE 8: Elemental atomic contents for the V_2O_5-xAg photocatalysts.

3.3.4. X-Ray Photoelectron Spectroscopy. Figure 8 shows the corresponding atomic contents of O, V, and Ag, determined from XPS, as a function of the Ag_2O load. From this figure, it is important to remark that the silver atomic content increases as the theoretical Ag_2O load increases. The spectrum region corresponding to V $2p_{3/2}$ has been only considered for the analysis. The corresponding V $2p_{3/2}$ core level spectra of vanadium pentoxide are depicted in Figure 9(a). The fitted

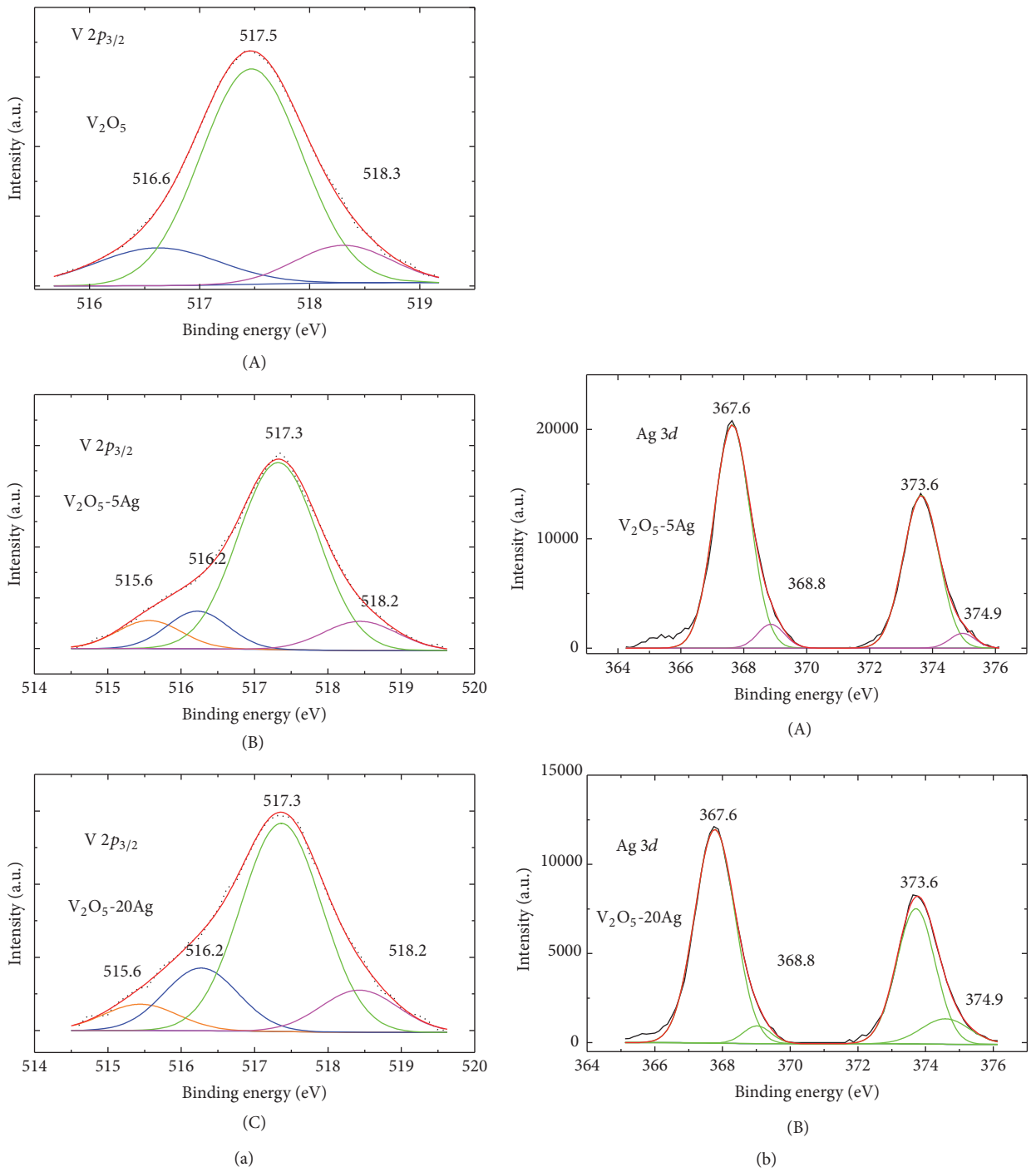

FIGURE 9: Core level spectra of (a) V $2p_{3/2}$ of (A) V_2O_5, (B) V_2O_5-5Ag, and (C) V_2O_5-20Ag and of (b) Ag $3d_{5/2}$ for (A) V_2O_5-5Ag and (B) V_2O_5-20Ag.

spectrum of the synthesized V_2O_5 shows binding energies at 515.6 and 517.5 eV. The peak at 515.6 eV is associated with V^{4+} species and the contribution at 517.5 eV corresponds to V^{5+} indicating the presence of V_2O_5 and confirming the Shcherbinaite crystalline structure observed by XRD. The incorporation of different Ag_2O loads into the photocatalytic formulation promotes the appearance of a new peak at binding energy of 516.2 eV, ascribed to the formation of the Ag-vanadium bronze ($Ag_{0.33}V_2O_5$) observed from XRD. Figures 9(a)(A)–(C) seem to indicate that the contribution at 516.2 eV increases with the Ag_2O loads. These results indicate that on the photocatalyst surfaces coexist mixed-valence vanadium oxides [41]. Concerning the fitting of the Ag $3d$ signal (Figure 9(b)), the contribution of two doublets is observed in all cases. One of them, centered at 367.7 and 373.6 eV, is attributed to the presence of Ag^+ species in the

Table 3: Band gap energy (E_g).

Catalyst	E_g (eV)	Wavelength (nm)
V_2O_5	2.3	564
V_2O_5-1Ag	2.2	566
V_2O_5-5Ag	1.6	765
V_2O_5-10Ag	1.4	867
V_2O_5-15Ag	1.2	1000
V_2O_5-20Ag	1.2	1033

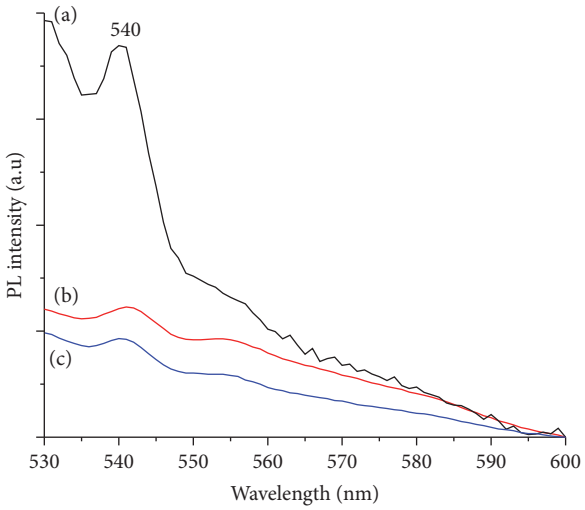

Figure 10: Photoluminescence spectra of (a) commercial V_2O_5, (b) synthesized V_2O_5, and (c) V_2O_5-20Ag.

$Ag_{0.33}V_2O_5$ oxide, while the other, centered at 368.8 and 374.9 eV, could be due to the presence of the Ag^+ species in Ag_2O, in agreement with the XRD results [41]. Finally, it should be mentioned that the O 1*s* spectra decrease slightly their intensity with the increase in atomic silver content and the characteristic peak is at 530.2 eV.

3.4. Band Gap Energy

3.4.1. Diffuse Reflectance Spectroscopy. It is well known that pentavalent vanadium has no d electrons and hence d-d transitions are not possible. Therefore, the observed bands in the electronic absorption spectrum are ascribed to charge transfer bands. The reflectance spectrum was processed with the Kubelka-Munk function and the optical band gap energy (E_g) was obtained as can be seen in Table 3. Results reveal that the increase in the Ag_2O load in photocatalytic formulation promotes narrowing of the band gap from 2.3 eV to values as low as 1.2 eV, remarking that this low band gap value makes this material potentially active under solar light.

3.4.2. Photoluminescence Spectroscopy. Figure 10 shows the photoluminescence spectra of the commercial and synthesized V_2O_5 as well as the V_2O_5-20Ag samples. The PL spectrum of the commercial V_2O_5 is characterized by an intense band peaking at 543. In contrast, the PL emission of the V_2O_5 obtained by the surfactant assisted technique shows

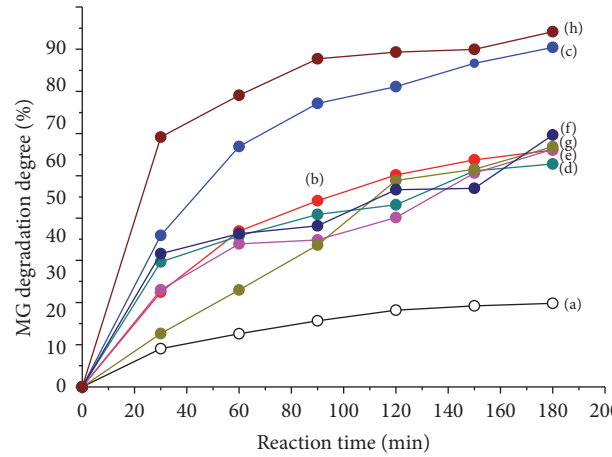

Figure 11: Photocatalytic degradation of malachite green dye during the first 180 minutes of reaction time (a) without catalyst (photolysis) and the photocatalytic process using (b) commercial V_2O_5, (c) synthesized V_2O_5, (d) V_2O_5-1Ag, (e) V_2O_5-5Ag, (f) V_2O_5-10Ag, (g) V_2O_5-15Ag, and (h) V_2O_5-20Ag photocatalysts.

the same band but with a lower intensity, almost three times less intensity. This can be interpreted as a higher electron-hole recombination rate in the commercial sample as the PL intensity is related directly to the recombination rate. An additional PL intensity decrease is also seen in the spectrum of the V_2O_5-20Ag photocatalyst, indicating that this sample exhibits the lowest recombination rate.

3.5. Photocatalytic Activity. Photocatalytic activity was evaluated in the degradation of the malachite green dye. Figure 11 shows that the photodegradation of the MG dye in the photolysis process is very low as can be seen in Figure 11(a). The use of the commercial V_2O_5 sample degrades 56% of the initial MG concentration after 180 min as is shown in Figure 11(b). The synthesized V_2O_5 catalyst (Figure 11(c)) reached a higher photocatalytic activity than the commercial sample, close to 80% of MG degradation. The Ag incorporation and further increase of the silver load in the photocatalyst decrease the photocatalytic activity in the range of 52–60% of MG degradation (Figures 11(d)–11(g)); however, the V_2O_5-20Ag photocatalyst exhibits the highest MG degradation reaching 84% (Figure 11(h)). It is worth noting that this is the best result found in this work, in which a photocatalyst that degrades organic molecules, as the MG dye, takes advantage of the cheapest illumination source as the sunlight. Moreover, a catalyst with high insolubility in water was obtained. This photocatalytic activity obtained was correlated with the acicular morphology of this material, which enhances the contact area in the reaction system. Also, the mixture of several semiconductors such as the V_2O_5, the $Ag_{0.33}V_2O_5$, and the small fraction of Ag_2O works as coupled conduction bands with electron transfer between them and decreases the recombination rate of the electron-hole pair, as was suggested by the photoluminescence results. Table 4 shows the reaction rate constant values k_{app} (min^{-1}) obtained from the fitting of the MG concentration at the early reaction times. Assuming a

Table 4: Kinetic rate constant (k_{app}) for photocatalytic formulations as a function of the silver load, determined using a nonlinear least squares data treatment [31].

Photocatalyst	% of degradation (UV-Vis)	% of degradation (TOC)	k_{app} (min^{-1})
V_2O_5	80.4	69.9	0.0081 ± 0.0001
V_2O_5-1Ag	52.8	67.5	0.0049 ± 0.0008
V_2O_5-5Ag	56.3	54.3	0.0056 ± 0.0007
V_2O_5-10Ag	56.9	56.0	0.0081 ± 0.0009
V_2O_5-15Ag	59.7	73.9	0.0053 ± 0.0001
V_2O_5-20Ag	84.2	74.4	0.0082 ± 0.0002

pseudo-first-order expression, a nonlinear least square fitting was used with an acceptable precision [31]. This reaction rate constant values agrees well with the degradation degree results. Additionally, the mineralization degree was followed by the quantification of the total organic carbon (TOC) through the reaction time; both results are quite similar as can be seen in Table 4, indicating that the photodegradation process follows the mineralization route of the organic dye tested.

4. Conclusions

Ag-modified photocatalysts were obtained in an easy way with acicular morphologies and enhanced specific surface areas. The changes in morphology and textural properties are associated with the appearance of new phases such as $Ag_{0.33}V_2O_5$ as well as Ag_2O coexisting at higher Ag loads as was suggested by XRD and XPS. These new phases have a strong influence in the photocatalytic response of these systems. It was observed that Ag incorporation into the photocatalytic formulation narrows the band gap energy making these materials photoactive under sunlight, a natural and cheaper irradiation source. The obtained photocatalytic formulations are conformed by a mixture of crystalline phases that work as coupled semiconductors. The V_2O_5-20Ag catalyst was the most active for the MG degradation using simulated sunlight.

Competing Interests

The authors declare that they have no competing interests.

Acknowledgments

The authors thank CONACyT for the financial support through CB-168827 and CB-240998 projects and CB-239648 project and also thank the academic staff of CCIQS Alejandra Núñez, Lizbeth Triana, Citlalit Martínez, and Dr. Uvaldo Hernández Balderas. E. Rodriguez Castellon and A. Infantes thank the financial support of the CTQ2015-68951-C3-3-R project (Ministerio de Economía y Competitividad) and FEDER funds.

References

[1] A. Fujishima and K. Honda, "Electrochemical photolysis of water at a semiconductor electrode," *Nature*, vol. 238, no. 5358, pp. 37–38, 1972.

[2] L. Di, H. Hajime, O. Naoki, H. Shunichi, and Y. Yukio, "Synthesis of nanosized nitrogen-containing MO_x-ZnO (M = W, V, Fe) composite powders by spray pyrolysis and their visible-light-driven photocatalysis in gas-phase acetaldehyde decomposition," *Catalysis Today*, vol. 93–95, pp. 895–901, 2004.

[3] I. N. M. Posada Velázquez, "Los compuestos orgánicos persistentes y su toxicidad a la salud humana," 2009, http://es.scribd.com/doc/16026795/Los-compuestos-organicos-persistentes-y-su-toxicidad-a-la-salud-humana.

[4] D. Dhananjay, S. Bhatkhande, V. G. Pangarkar, and A. Beenackers, "Photocatalytic degradation for environmental applications—a review," *Journal of Chemical Technology and Biotechnology*, vol. 77, no. 1, pp. 102–116, 2002.

[5] A. I. Martínez, D. Acosta, and A. López, "Efecto del contenido de Sn sobre las propiedades físicas de películas delgadas de TiO_2," *Superficies y Vacío*, vol. 16, pp. 5–9, 2003.

[6] K. Melghit, A. K. Mohammed, and I. Al-Amri, "Chimie douce preparation, characterization and photocatalytic activity of nanocrystalline SnO_2," *Materials Science and Engineering B: Solid-State Materials for Advanced Technology*, vol. 117, no. 3, pp. 302–306, 2005.

[7] H. T. Tran, H. Kosslick, M. F. Ibad et al., "Photocatalytic performance of highly active brookite in the degradation of hazardous organic compounds compared to anatase and rutile," *Applied Catalysis B: Environmental*, vol. 200, pp. 647–658, 2017.

[8] S. Chen, D. Li, Y. Liu, and W. Huang, "Morphology-dependent defect structures and photocatalytic performance of hydrogenated anatase TiO_2 nanocrystals," *Journal of Catalysis*, vol. 341, pp. 126–135, 2016.

[9] K. Nakata and A. Fujishima, "TiO_2 photocatalysis: design and applications," *Journal of Photochemistry and Photobiology C: Photochemistry Reviews*, vol. 13, no. 3, pp. 169–189, 2012.

[10] C. McManamon, J. O'Connell, P. Delaney, S. Rasappa, J. D. Holmes, and M. A. Morris, "A facile route to synthesis of S-doped TiO_2 nanoparticles for photocatalytic activity," *Journal of Molecular Catalysis A: Chemical*, vol. 406, pp. 51–57, 2015.

[11] H. Li, G. Zhao, G. Han, and B. Song, "Hydrophilicity and photocatalysis of $Ti_{1-x}V_xO_2$ films prepared by sol-gel method," *Surface and Coatings Technology*, vol. 201, no. 18, pp. 7615–7618, 2007.

[12] T. Bak, J. Nowotny, M. Rekas, and C. C. Sorrell, "Photo-electrochemical hydrogen generation from water using solar energy. Materials-related aspects," *International Journal of Hydrogen Energy*, vol. 27, no. 10, pp. 991–1022, 2002.

[13] X. Yong and M. A. A. Schoonen, "The absolute energy positions of conduction and valence bands of selected semiconducting minerals," *American Mineralogist*, vol. 85, no. 3-4, pp. 543–556, 2000.

[14] F. Amano, M. Tanaka, and B. Ohtani, "Alkali metal ion-modified vanadium mononuclear complex for photocatalytic mineralization of organic compounds," *Catalysis Letters*, vol. 140, no. 1, pp. 27–31, 2010.

[15] M. A. Rauf, S. B. Bukallah, A. Hamadi, A. Sulaiman, and F. Hammadi, "The effect of operational parameters on the photoinduced decoloration of dyes using a hybrid catalyst V_2O_5/TiO_2," *Chemical Engineering Journal*, vol. 129, no. 1-3, pp. 167–172, 2007.

[16] K. Teramura, T. Tanaka, M. Kani, T. Hosokawa, and T. Funabiki, "Selective photo-oxidation of neat cyclohexane in the liquid phase over V_2O_5/Al_2O_3," *Journal of Molecular Catalysis A: Chemical*, vol. 208, no. 1-2, pp. 299–305, 2004.

[17] C. Karunakaran and P. Anilkumar, "Photooxidation of iodide ion on immobilized semiconductor powders," *Solar Energy Materials and Solar Cells*, vol. 92, no. 4, pp. 490–494, 2008.

[18] X. Rui, Y. Tang, O. I. Malyi et al., "Ambient dissolution-recrystallization towards large-scale preparation of V_2O_5 nanobelts for high-energy battery applications," *Nano Energy*, vol. 22, pp. 583–593, 2016.

[19] J. Mu, J. Wang, J. Hao et al., "Hydrothermal synthesis and electrochemical properties of V_2O_5 nanomaterials with different dimensions," *Ceramics International*, vol. 41, no. 10, pp. 12626–12632, 2015.

[20] H. He, L. Zan, and Y. Zhang, "Effects of amorphous V_2O_5 coating on the electrochemical properties of $Li[Li_{0.2}Mn_{0.54}Ni_{0.13}Co_{0.13}]O_2$ as cathode material for Li-ion batteries," *Journal of Alloys and Compounds*, vol. 680, pp. 95–104, 2016.

[21] S. Sel, O. Duygulu, U. Kadiroglu, and N. E. Machin, "Synthesis and characterization of nano-V_2O_5 by flame spray pyrolysis, and its cathodic performance in Li-ion rechargeable batteries," *Applied Surface Science*, vol. 318, pp. 150–156, 2014.

[22] A. A. Mane, V. V. Ganbavle, M. A. Gaikwad, S. S. Nikam, K. Y. Rajpure, and A. V. Moholkar, "Physicochemical properties of sprayed V_2O_5 thin films: effect of substrate temperature," *Journal of Analytical and Applied Pyrolysis*, vol. 115, pp. 57–65, 2015.

[23] C. Julien, E. Haro-Poniatowski, M. A. Camacho-López, L. Escobar-Alarcón, and J. Jímenez-Jarquín, "Growth of V_2O_5 thin films by pulsed laser deposition and their applications in lithium microbatteries," *Materials Science and Engineering B*, vol. 65, no. 3, pp. 170–176, 1999.

[24] F. Gonzalez-Zavala, L. Escobar-Alarcón, D. A. Solís-Casados, C. Rivera-Rodríguez, R. Basurto, and E. Haro-Poniatowski, "Preparation of vanadium oxide thin films modified with Ag using a hybrid deposition configuration," *Applied Physics A: Materials Science and Processing*, vol. 122, no. 4, article 461, 2016.

[25] N. Serpone and E. Pelizzetti, *Photocatalysis: Fundamentals and Applications*, John Wiley & Sons, New York, NY, USA, 1989.

[26] D. Bahnemann, "Photocatalytic water treatment: solar energy applications," *Solar Energy*, vol. 77, no. 5, pp. 445–459, 2004.

[27] Y. He, Y. Wu, T. Sheng, and X. Wu, "Photodegradation of acetone over V-Gd-O composite catalysts under visible light," *Journal of Hazardous Materials*, vol. 180, no. 1-3, pp. 675–682, 2010.

[28] T. Ishihara, N. S. Baik, N. Ono, H. Nishiguchi, and Y. Takita, "Effects of crystal structure on photolysis of H_2O on K–Ta mixed oxide," *Journal of Photochemistry and Photobiology A: Chemistry*, vol. 167, no. 2-3, pp. 149–157, 2004.

[29] T. Ohno, S. Izumi, K. Fujihara, and M. Matsumura, "Electron-hole recombination via reactive intermediates formed on PdO-doped $SrTiO_3$ electrodes. Estimation from comparison of photoluminescence and photocurrent," *Journal of Photochemistry and Photobiology A: Chemistry*, vol. 129, no. 3, pp. 143–146, 1999.

[30] F. Han, V. S. R. Kambala, M. Srinivasan, D. Rajarathnam, and R. Naidu, "Tailored titanium dioxide photocatalysts for the degradation of organic dyes in wastewater treatment: a review," *Applied Catalysis A: General*, vol. 359, no. 1-2, pp. 25–40, 2009.

[31] G. Lente, *Deterministic Kinetics in Chemistry and Systems Biology*, Springer, 2015.

[32] A. B. Murphy, "Band-gap determination from diffuse reflectance measurements of semiconductor films, and application to photoelectrochemical water-splitting," *Solar Energy Materials and Solar Cells*, vol. 91, no. 14, pp. 1326–1337, 2007.

[33] R. López and R. Gómez, "Band-gap energy estimation from diffuse reflectance measurements on sol-gel and commercial TiO_2: A Comparative Study," *Journal of Sol-Gel Science and Technology*, vol. 61, no. 1, pp. 1–7, 2012.

[34] P. Malathy, K. Vignesh, M. Rajarajan, and A. Suganthi, "Enhanced photocatalytic performance of transition metal doped Bi_2O_3 nanoparticles under visible light irradiation," *Ceramics International*, vol. 40, no. 1, pp. 101–107, 2014.

[35] D. Solís, E. Vigueras-Santiago, S. Hernández-López, A. Gómez-Cortés, M. Aguilar-Franco, and M. A. Camacho-López, "Textural, structural and electrical properties of TiO_2 nanoparticles using Brij 35 and P123 as surfactants," *Science and Technology of Advanced Materials*, vol. 9, no. 2, 2008.

[36] J. M. Lee, H.-S. Hwang, W.-I. Cho, B.-W. Cho, and K. Y. Kim, "Effect of silver co-sputtering on amorphous V_2O_5 thin-films for microbatteries," *Journal of Power Sources*, vol. 136, no. 2, pp. 122–131, 2004.

[37] T. Ono, Y. Tanaka, T. Takeuchi, and K. Yamamoto, "Characterization of K-mixed V_2O_5 catalyst and oxidative dehydrogenation of propane on it," *Journal of Molecular Catalysis A: Chemical*, vol. 159, no. 2, pp. 293–300, 2000.

[38] Libro, "Tablas para la elucidación estructural de compuestos orgánicos por métodos espectroscópicos".

[39] M. D. Soriano, A. Vidal-Moya, E. Rodríguez-Castellón, F. V. Melo, M. T. Blasco, and J. M. López-Nieto, "Partial oxidation of hydrogen sulfide to sulfur over vanadium oxides bronzes," *Catalysis Today*, vol. 259, pp. 237–244, 2016.

[40] J. C. Badot, D. G. F. Bourdeau, N. Baffier, and A. Tabuteau, "Electronic Properties of $Na_{0.33}V_2O_5$ bronze obtained by sol-gel process," *Journal of Solid State Chemistry*, vol. 92, pp. 8–17, 1991.

[41] M. E. Tousley, A. W. Wren, M. R. Towler, and N. P. Mellott, "Processing, characterization, and bactericidal activity of undoped and silver-doped vanadium oxides," *Materials Chemistry and Physics*, vol. 137, no. 2, pp. 596–603, 2012.